Diffraction Suppression Technique for Background Images in Curved Transparent Displays

Yu-Hung Wang, Yu-Wen Wang, Nehemiah Chuanfeng Kuo, and Hoang-Yan Lin
Graduate Institute of Photonics and Optoelectronics, National Taiwan University, Taipei 106, Taiwan

Abstract
By integrating an inverse propagation phase retrieval algorithm with a customized simulated annealing (SA) algorithm, this research designed Diffractive Optical Elements (DOEs) to suppress unwanted diffraction spots in curved transparent displays. Results show that the proposed method increases the zero-order diffraction ratio from 42.261% to 65.752%, offering a scalable solution for curved transparent displays in automotive, AR/VR, and under-display camera applications.

Keywords
curved transparent displays; phase retrieval algorithm; simulated annealing algorithm; Fresnel diffraction; diffractive optical elements.

1. Introduction
Transparent displays are crucial in applications such as augmented reality (AR), automotive head-up displays (HUDs), and under-display cameras (UDCs). In automotive or window transparent displays, curved panel designs are often adopted to suit the vehicle design or enhance the user's immersive experience. The curvature not only integrates seamlessly with overall design aesthetics but also effectively reduces aberrations and optical distortions. Moreover, curved transparent displays enhance visibility by reducing glare and reflection, while their wider field of view improves depth perception. However, the application of self-emissive transparent displays remains limited by diffraction caused by heterogeneous structures, which disrupts the quality of background images. This issue is particularly critical in automotive transparent displays, where clear background images are essential for driving safety.

To address this challenge, we propose a novel and efficient phase retrieval algorithm, implemented through dynamic programming. This algorithm is designed to find a phase distribution matrix that performs a convolution with the incident light field to approximate the target light field without diffraction. Additionally, we develop a customized simulated annealing algorithm that conducts a global search to achieve the optimal solution while reducing computational complexity and maintaining high precision. By modifying the point spread function using these algorithms, the degradation caused by diffraction in the imaging process can be effectively reduced.

2. Theory

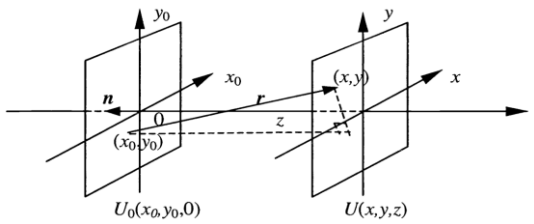

Figure 1. The coordinate system for diffraction calculation.

$$U(x,y,z)=\int_{-\infty}^{\infty}\int_{-\infty}^{\infty}U_0(x_0,y_0,0)\frac{\exp\left(jk\sqrt{z^2+(x-x_0)^2+(y-y_0)^2}\right)}{j\lambda\sqrt{z^2+(x-x_0)^2+(y-y_0)^2}}\times\left(\frac{1}{2}+\frac{z}{2\sqrt{z^2+(x-x_0)^2+(y-y_0)^2}}\right)dx_0dy_0 \quad (1)$$

In automotive windshield applications, due to the curvature of the windshield, the light propagation distance **z** is no longer constant and varies with the x-y coordinates of the matrix, expressed as z(x, y)**,** as shown in Fig. 1. An increase in curvature may leading to greater phase variation frequencies. To simulate the field distribution after light passes through the curved electrode structure, this study employs the Fresnel-Kirchhoff diffraction formula [1] and the two-step diffraction propagation technique [2]. Here, the output light field U is represented as the convolution of the incident light field U_0 and the impulse response h (x, y)**,** as given by Eq. (1). When the curvature is relatively small, the impulse response h (x, y) can be approximated as a space-invariant system in z-direction, where its characteristics depend only on the relative distance between the two planes.

3. Modeling
Since the automotive windshield parameters are often commercial secrets, we used the built-in HUD windshield model in Zemax® and extracted its parameters. The windshield is represented as an extended polynomial surface of a non-spherical shape, the polynomial is shown in Eq. (2)[3].

$$z=\frac{cr^2}{1+\sqrt{1-(1+k)c^2r^2}}+\sum_{i=1}^{N}A_iE_i(x,y) \quad (2)$$

The parameter c represents the curvature, while r is the radial distance, defined as $r=\sqrt{x^2+y^2}$, indicating the distance from the surface center to a specific point, and k represents conic constant. The higher-order coefficients Ai are used to adjust the non-spherical terms of the surface. Additionally, $Ei(x,y)$ defines the surface variation in the (x,y) directions.

Since the electrode size is of the micron scale and the wavelength is of the nanometer scale, according to the Nyquist–Shannon sampling theorem, the sampling grid number must be greater than 2 × (sampling range / wavelength λ). Simulating an entire windshield (1m × 2m) is impractical due to hardware limitations (256GB RAM). Therefore, using the extracted parameters to simulate the surface within a small sample area (1.75cm×1.75cm) is more practical and realistic.

The fitting surface parameters flowchart is shown in Fig. 2, the process begins by opening the file and reading the number of faces. Space is pre-allocated to store the face data, including the vertices and face indices. For each face, the coordinates of its three vertices are read and stored sequentially in the vertices list, while the indices of these vertices are saved in the face data structure. Once all the data is processed, the three-dimensional coordinates of the vertices are extracted.

ISSN 0097-996X/25/5602-0760-$1.00 © 2025

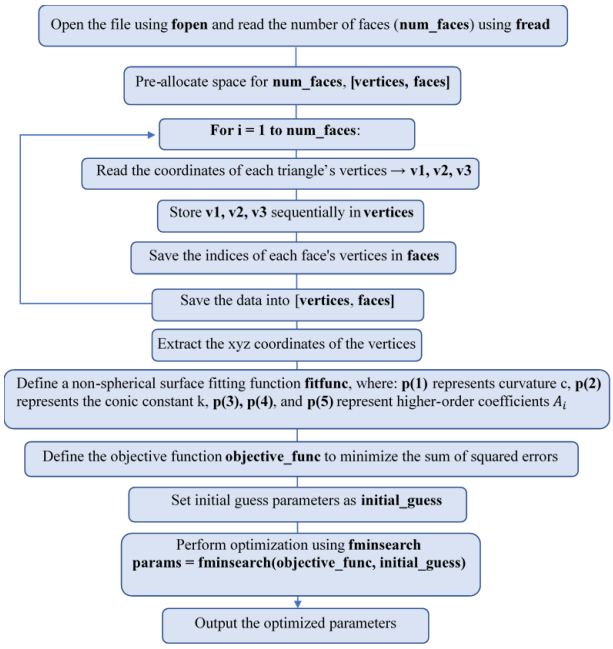

Figure 2. Fitting Surface Parameters Flowchart.

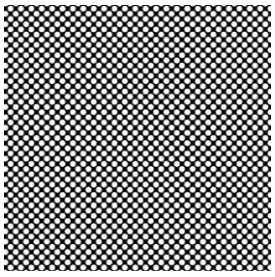

Figure 3. Pixel structure of planar transparent display.

In Fig. 3, the aperture structure [4] of a planar transparent display is shown, where the circular regions represent the display's apertures, while the other areas correspond to the opaque electrode regions. With the extracted parameters from the windshield model and the pixel structure, we can use them to model a transparent windshield display structure, as shown in Fig. 4, to simulate the light field propagation.

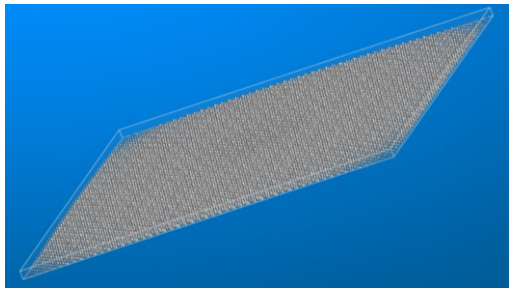

Figure 4. The transparent windshield display model.

4. Simulation and Algorithm

4.1. Optical Theories of Diffraction

Optical simulation software MATLAB® is utilized for model construction. To simulate the field distribution after light passes through the curved electrode structure, the two-step diffraction propagation technique mentioned in the book "*Computational Fourier Optics: A MATLAB Tutorial*" [2] is employed. This technique decomposes the propagation path into multiple segments of free-space propagation for simulation. In this study, the Fresnel-Kirchhoff diffraction formula without paraxial approximation is used. U_0 represents the field before entering the transparent panel, as given by Eq. (3).

$$U_0 = \exp(ikR(x,y,z)) / R(x,y,z) \quad (3)$$

However, after passing through the panel, it is necessary to account for the phase difference caused by the opaque electrodes on the panel. Thus, the incident light field U_0 needs to be multiplied by the mask and phase distribution matrix to obtain the field U_{in} after exiting the heterogeneous structure, which is shown in Eq. (4).

$$U_{in} = U_0 * \text{mask} * \text{phase} \quad (4)$$

After passing through a glass panel with a thickness of z_1, Fresnel-Kirchhoff diffraction can be regarded as the convolution of U_{in} with the impulse response function h, as given by Eq. (5)

$$U_{mask} = U_{in} \otimes h_{(z=z1)} \quad (5)$$

To facilitate the observation of the point spread function distribution, a lens with a focal length f is placed behind the panel, introducing a phase correction $Lens_{phase}$. Imaging is performed at $z_2=1/(1/f-1/z_0)$. As the light field exits the opposite surface of the substrate, it undergoes phase correction by the microstructures on the surface, represented as DOE. This results in the final light field U_f, as shown in Eq. (6).

$$U_f = (U_{mask} * \text{DOE} * Lens_{phase}) \otimes h_{(z=z2)} \quad (6)$$

Through forward and inverse Fourier transforms, the final imaging light field U_f is obtained, as shown in Fig. 5(a). Fig. 5(b) illustrates the ideal imaging result after removing the surrounding high-order diffraction patterns, which we define as the target field.

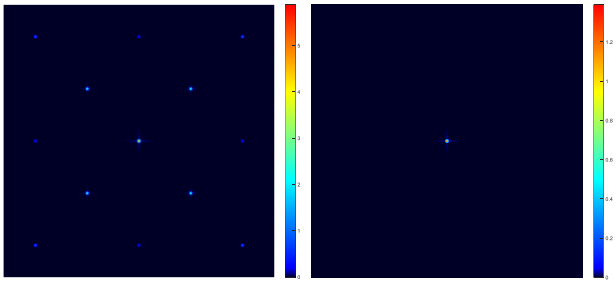

(a) (b)

Figure 5. (a) The diffraction light field of U_f. (b) The defined ideal target field.

4.2. Algorithm

To address the optical issues caused by diffraction, we adopt phase retrieval algorithms and simulated annealing as core methods [5] to overcome the limitations of traditional IFTA algorithms, such as susceptibility to local optima and errors caused by paraxial approximations. Phase modulation is employed for component design and optimization. Initially, the phase distribution is set to a zero matrix as the starting parameter for the diffraction suppression

element (DOE). Through iterative adjustments of the DOE phase matrix, the output field U_f is progressively brought closer to the target field U_{target}. The root mean square error (RMSE) is used as the evaluation metric, with the cost function defined as Eq. (7):

$$\text{Cost function} = \sqrt{\sum\sum(|U_f| - U_{target})^2} \cdot dx \cdot dy \qquad (7)$$

This metric quantifies the difference between the initial and target imaging. During the simulated annealing process, in addition to searching for the global optimal solution, the inner loop also performs local phase optimization, iteratively refining the phase distribution within submatrices to improve the cost function value. If the RMS error decreases, the phase matrix is updated, further approaching the optimization goal. To enhance efficiency, the study employs vectorization within this loop, enabling local updates, convolution, and evaluation calculations to be performed simultaneously. This reduces loop runtime, significantly improves efficiency, and accelerates convergence. The loop will stop when the convergence success rate reaches 99%, indicating that most perturbation steps effectively improve or maintain the objective function value, as shown in Fig. 6(a). The final results demonstrate that, after multiple iterations, the cost function converges to its minimum value, as shown in Fig. 6(b).

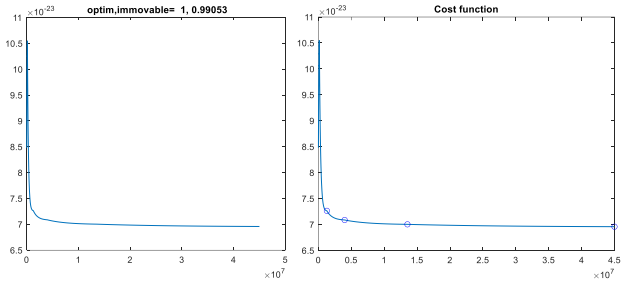

Figure 6. (a) The optimization of U_f. (b) Converge curve of the cost function.

4.3. Diffractive Optical Elements

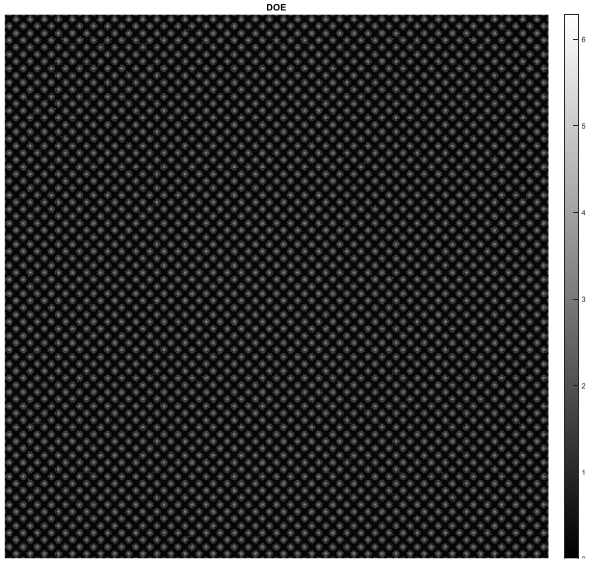

Figure7. Diffractive optical elements of curved transparent display.

Fig. 7 shows the designed diffraction suppression element, exhibiting a phase complementary effect between the pseudo-panel and the suppression element. The compensated areas of the resemble element and the suppression element are offset from each other. In the resemble element, certain areas are designed with phase compensation, while in regions without compensation, the suppression element introduces microstructures to provide the necessary compensation. This design ensures uniformity in the light field distribution.

5. Result & Discussion

5.1. Comparison of Diffraction Ratio

According to The Law of Energy Conservation, the total energy of the peripheral diffraction combined with the total energy of the central zero-order diffraction equals the total energy entering the panel. To suppress peripheral diffraction, it is necessary to further enhance the energy of the central zero-order diffraction. To evaluate the optimization effect, we use the diffraction ratio, defined as:

$$\text{Diffraction Ratio for n-th Order} = \frac{E_n}{E_{total}} \qquad (8)$$

Where E_n represents the total energy of each order diffraction spot, and E_{total} represents the total energy entering to the panel.

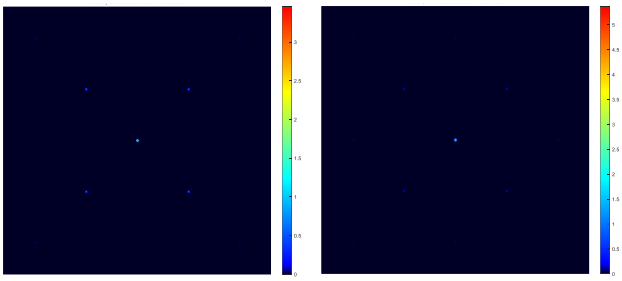

(a) (b)

Figure8. (a) The light field before optimization. (b) The light field after optimization.

Table 1. Comparison of zero-order Diffraction ratios

	$U_{initial}$	$U_{optimization}$
0^{th} order diffraction ratio	42.261%	65.752%

As observed, the zero-order diffraction ratio before optimization is 42.261%. After applying our algorithm, this value increases by 23.491%, reaching 65.752%. Subsequently, we examine the cross-sectional profile in the next section.

5.2. Cross-sectional profile analysis

To quantify and examine the intensity of the point spread function (PSF), we utilized intensity cross-section profile plots to observe the distribution and variation of the diffraction ratio. These plots provide a visual representation of how the energy is distributed across different diffraction orders and how optimization impacts the energy reallocation.

In the next two subsections, Fig. 9(a)(b) present the intensity distribution along the diagonal cross-section before and after optimization, while Fig. 10(a)(b) show the intensity distribution along the y-axis cross-section under the same conditions. The horizontal axis represents the positional coordinates, indicating the actual locations of each order diffraction spot. The vertical axis represents the amplitude, illustrating the intensity of each order's energy and whether the high-order energy has been redirected back to the zero-order through phase modulation. This analysis demonstrates the effectiveness of the optimization in redistributing energy and suppressing unwanted diffraction.

5.2.1. Diagonal Cross-Section Plot

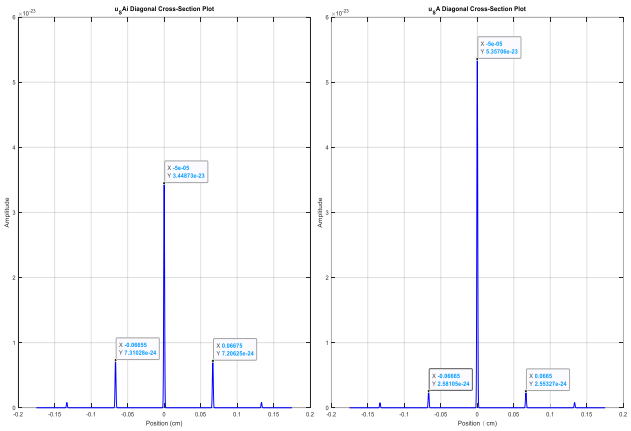

(a) (b)

Figure 9. (a) Diagonal Cross-Section Plot of $U_{initial}$. (b) Diagonal Cross-Section Plot of $U_{optimization}$.

5.2.2. Y-Axis Cross-Section Plot

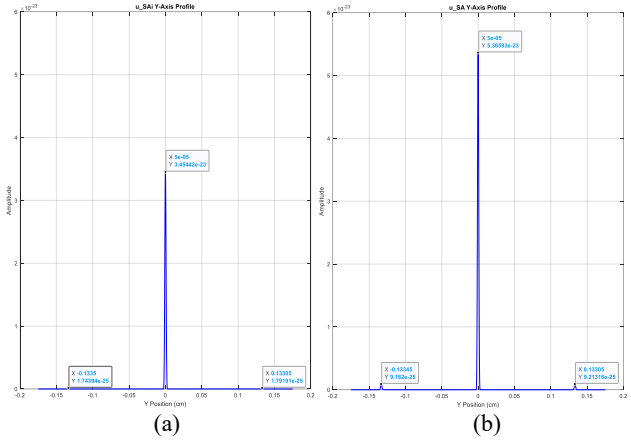

(a) (b)

Figure 10. (a) Y-Axis Cross-Section Plot of $U_{initial}$. (b) Y-Axis Cross-Section Plot of $U_{optimization}$.

5.3. Discussion

In the four cross-sectional plots, Fig. 9(a)(b) show the intensity along the diagonal cross-section before and after optimization, respectively, representing the diffraction intensity of the second-order diffraction spots. Similarly, Fig. 10(a)(b) show the intensity along the y-axis cross-section before and after optimization, respectively, representing the diffraction intensity of the first-order diffraction spots. When switch to diffraction ratios, the results can be observed in Table 2.

Table 2. Comparison of different order Diffraction ratios.

	$U_{initial}$	$U_{optimization}$
1st order diffraction ratio	0.219%	1.12%
2nd order diffraction ratio	8.958%	3.133%

We can see that the second-order diffraction ratio decreased by 5.825% (each diffraction spot), which is a significant optimization and explains the source of the substantial increase in the zero-order diffraction ratio. However, the first-order diffraction ratio increased by 0.901%. This result indicates that during the optimization process, part of the energy was redirected from the second-order diffraction to the zero-order, but some energy also shifted to the first-order diffraction. This suggests that future designs of diffraction suppression elements should focus on more precise energy redistribution, further suppressing both first-order and higher-order diffraction to achieve optimal optical performance.

6. Conclusions

This study addressed the issue of diffraction suppression in curved transparent displays caused by surface heterostructures. By integrating an inverse propagation phase retrieval algorithm with a customized simulated annealing (SA) algorithm, we successfully optimized Diffractive Optical Elements (DOEs) to reduce diffraction effects.

Through iterative optimization, the cost function demonstrated a consistent convergence trend, reaching 99% of the target distribution after tens of thousands of iterations. This optimization effectively redistributed energy, leading to an improvement in the zero-order diffraction ratio from 42.261% to 65.752%, along with a significant 5.825% reduction in the diffraction ratio for each second-order diffraction spot, which contributed to an increase in zero-order diffraction energy.

This study demonstrates the feasibility and effectiveness of phase modulation for diffraction suppression in curved transparent displays. Future work will focus on addressing residual diffraction effects, improving manufacturing compatibility, and exploring real-world applications such as automotive displays and AR/VR systems.

7. References

1. Goodman J.W., "*Introduction to Fourier Optics*" *2nd ed*., McGraw-Hill, New York; 2002.
2. Voelz D.G., "*Computational Fourier Optics: A MATLAB Tutorial*", Bellingham (WA): SPIE; 2011.
3. Wei S., Fan Z., Zhu Z., and Ma D., Design of a head-up display based on freeform reflective systems for automotive applications. Applied Optics, vol. 58, no. 7, pp. 1675–1681, 2019.
4. Tsai Y.H., Huang M.H., Huang T.W., Lo K.L., Ou-Yang M. Image quality affected by diffraction of aperture structure arrangement in transparent active-matrix organic light-emitting diode displays. Applied optics. Oct1;54(28):E136-E145, 2015.
5. Chen Y.X., Reverse Propagation Phase Retrieval Algorithm for the Diffraction Inhibiting Optical Element of Under Display Camera [Master's thesis]. Taipei (Taiwan): National Taiwan University; 2022. Available from: https://doi.org/10.6342/NTU202204166